Natural Hazards (2005) 35: 321–342
DOI 10.1007/s11069-004-1795-4

Modelling and Mapping Damage to Forests from an Ice Storm Using Remote Sensing and Environmental Data

D. J. KING [1,★], I. OLTHOF[1], P. K. E. PELLIKKA[2], E. D. SEED[1] and C. BUTSON[1]
[1]*Department of Geography and Environmental Studies, Carleton University, 1125 Colonel By Drive, Ottawa, Ontario, Canada KIS 5B6;* [2]*Department of Geography, University of Helsinki, Finland*

(Final version accepted: 10 February 2004)

Abstract. An extreme ice storm in January 1998 deposited up to 100 mm of ice and resulted in significant forest damage across eastern North America. Average crown loss of over 75% was recorded in large areas of eastern Ontario and southern Quebec. A primary question that arose following the storm was: can forest damage be effectively assessed using remote sensing and other available environmental data? This paper presents two contrasting studies to address this question. The first involves damage modelling at a local scale in an unmanaged forest using spectral and spatial information in high-resolution airborne imagery. Results of field data analyses are also given that show relations between damage and forest structure and composition as well as changes in forest structure that occurred in the years following the storm. The second study involves regional scale damage mapping in managed and unmanaged forests of eastern Ontario using medium resolution satellite imagery and other environmental data. In comparison of several image classification and data interpolation methods, the best damage map was produced using a neural network classifier and a mix of Landsat and environmental data. The methods and results presented in this paper form the basis for ongoing long-term temporal study of damage impacts on forest condition.

Keywords: ice storm, forest damage, remote sensing and environmental data, spectral and spatial image analysis

1. Introduction

Forest ecosystems worldwide are undergoing significant changes from natural and anthropogenic disturbances. Impacts are evident at a wide range of scales from the biome level (Canadian Institute of Forestry, 2000) to individual stands and trees (Mageau *et al.*, 1995). Forest disturbance (including management effects) is increasing in frequency and magnitude due to factors such as climate change, increasing demand for forest products, and land

★ Author for correspondence: E-mail: doug.king@carleton.ca

conversion to urban or agricultural uses. This impacts forest ecology, forest management (Parker *et al.*, 2000) and floral and faunal habitat (Ehrlich, 1995). Efforts are being made to develop methods for sustainable management of forests to reduce adverse impacts while maintaining adequate productivity for human use. Measurement and monitoring components of these efforts include the system of "Criteria and Indicators" as stipulated in the Montreal Process (Canadian Council of Forest Ministers, 1995), many of these being suitable for measurement using geo-spatial data and analytical techniques (Goodenough *et al.*, 1998). Franklin (2000) summarizes them within a detailed treatment of the context and methods of remote sensing in sustainable forestry. Disturbance assessment and monitoring are significant aspects of sustainable management and of efforts to improve our knowledge of ecological processes. Robust methods are needed to quantify and map impacts resulting from various disturbance types including long-term stress, sudden high impact stress, or forest management operations. The research programme at Carleton University (King, 2002) addresses each of these using multi-scale remote sensing and environmental data analysis. For the purposes of this special issue, this paper focuses on the high impact forest disturbance that resulted from the 1998 ice storm of eastern North America.

1.1. THE 1998 ICE STORM

Ice storms typically result when a moist warm air mass overrides a colder air mass that is situated over a frozen ground surface (Oliver and Larson, 1996). Rainfall freezes on impact causing ice accretion on surfaces. Ice storms generally occur with high frequency (every 20–100 years) in the eastern United States and the region from eastern Ontario to the Atlantic Provinces of Canada (Smith, 1998). Most storms only cover small areas within these regions, but local accumulation of ice can be significant, causing downed hydro lines and breakage of tree branches or trunks. They are one of the few recurring regional scale natural phenomena in eastern temperate forests that are responsible for damaging trees. However, forest response and adaptation to such damage has not been rigorously studied over the long-term (Stabb, 1998). Irland (1998) states that survival chances vary from good for crown loss of less than 50%, to unlikely for crown loss greater than 75%. At higher levels of damage, growth suppression and wood degradation are also expected. When trees lose branches, energy is focused on the development of dormant buds and new branches. This may cause a reduction in root development, diameter growth and defensive compound synthesis, which in turn may cause soil moisture stress and an increased susceptibility to disease and insect infestation (Irland, 1998; Coons, 1999; Boulet *et al.*, 2000). For managed forests, there is significant possibility of further decline in forest value as insects or fungi invade large wounds (Smith, 1998). Changes in

successional dynamics may also occur in the understory layers in response to increased light penetration resulting in increased competition for nutrients and moisture (Aber and Mollillo, 1991).

Between January 4th and 9th, 1998 up to 100 mm of freezing rain fell in eastern Canada and the north eastern United States. The area of ice accumulation was approximately 10 million hectares, although forest damage was highly variable and patchy. Forest biomass loss in severely affected areas was greater than that measured in several recent hurricanes (Hooper *et al*., 2001). A storm of such magnitude and spatial extent is estimated to have a return period of at least 500 years (Smith, 1998). Ontario Ministry of Natural Resources (OMNR) sketch mapping of damage by helicopter found it to be most consistently severe in the central portion of eastern Ontario (Figure 1, http://www.eomf.on.ca/ISFRATT/maps.htm).

In some small areas, all tree trunks had been snapped, while in others, trees were bent in an arc with their crowns frozen at ground level or held by other tree crowns. Over large areas, damage consisted more of broken branches (Figure 2) and tree bending or lean. Due to the magnitude of damage, both ecologically and economically, questions arose whether ice storm damage could be assessed and mapped more objectively using remote sensing, and other available environmental data.

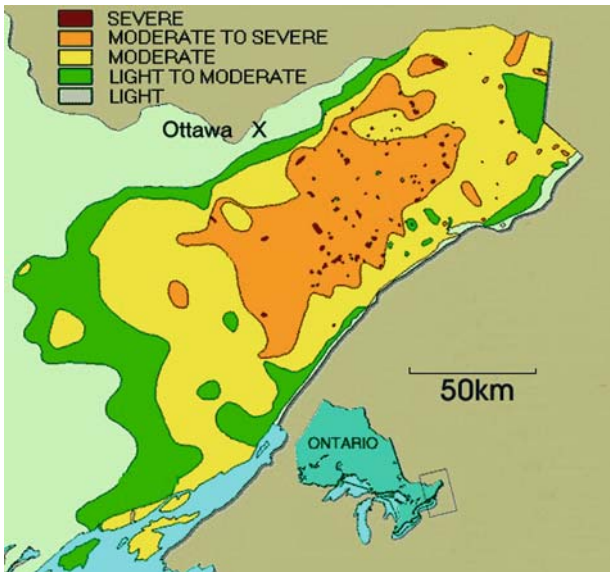

Figure 1. Sketch map of forest damage in eastern Ontario produced from low altitude airborne survey following the ice storm.

Figure 2. Moderate to severe damage in a sugar maple forest, May 1998.

1.2. MODELLING AND MAPPING OF FOREST CHANGE USING REMOTE SENSING

Remote sensing for assessment of forest damage from insects and disease, and modelling of forest structure variations in natural and managed conditions have been well researched. Traditional approaches to vegetation damage assessment with remote sensing have included either visual analysis of aerial photography (e.g., Hall *et al.*, 1993) or multispectral analysis of digital imagery (e.g., Leckie *et al.*, 1992). Spectral analysis techniques have advanced significantly, and capabilities for detection of physiological indicators of stress (e.g., OMNR, 1997; Sampson *et al.*, 2000) are being developed. However, analysis of spectral symptoms alone does not capture the variability in forest structure caused by disturbance. Forest structure assessment using remote sensing is best conducted with both spectral and spatial image information, although the latter has not received as much attention in the literature as the former. Image spatial measures such as texture (e.g., Wulder *et al.*, 1998; Olthof and King, 2000), semivariance parameters (e.g., Bowers *et al.*, 1994; Lévesque and King, 1999; Sampson *et al.*, 2001), and image fractions (e.g., Peddle *et al.*, 1999; Lévesque and King, 2003) have been found to be useful for forest structure modelling and, in some cases, forest damage. Most of these studies, though, have been concerned with prediction of single forest variables. Some recent work has integrated concepts of multivariate representation of forest structure condition as a score or index composed of

several forest variables. This integrated approach to quantitative forest assessment is more ecologically relevant and is gaining increased attention in the research community (e.g., Jakubauskas (1996) for forest structure; Olthof and King (2000), Cosmopoulos and King (2004) for forest health in a contaminated and windblown environment; Coops *et al*. (2001) for Australian forest condition).

2. Objectives

This paper presents remote sensing and environmental data modelling and mapping of ice storm forest damage. They are part of a long-term programme to monitor forest response to the ice storm of 1998 and to aid in development of understanding of the types, magnitude, and spatial patterns of change that result from such events. Two studies that contrast in goals, scales, data and methods are described. Study 1, in a protected park in southern Quebec, is a local scale analysis of damage modelling using high-resolution airborne imagery. Study 2, in eastern Ontario, is a regional scale analysis of damage mapping in managed and unmanaged forests that compares classification of geo-spatial data with interpolation from a dense network of field damage estimates.

For the purpose of this special issue, the paper focuses on the questions: What are ice storm impacts on forests and how can we model or map these using remote sensing and environmental data? For the latter, two of the primary methodologies that are used in remote sensing, biophysical modelling and classification, are summarized. These methodologies are also applicable to forest structure mapping in other disturbance conditions or in undisturbed conditions when it is desired to quantify forest structure variation for some other purpose (e.g. forest management). Specific aspects of this research such as the use of low cost high-resolution imagery and the integration of image spectral and spatial information, landscape metrics and environmental data are less common in the literature as they are still relatively recent.

3. Study 1: Local Scale Analysis of Forest Ice Storm Damage

Forests that are not managed for extractive purposes present an opportunity to study and monitor short and long-term impacts of a disturbance such as the 1998 ice storm. The study site is centred at 45°30'N, 75°52'W in the Gatineau Park, a temperate hardwood forest of about 10×50 km northwest of Ottawa (Figure 3). The dominant overstory species in the park is sugar maple (*Acer saccharum* Marsh.), but there are small patches dominated by American beech (*Fagus grandifolia* Ehrh.), trembling aspen (*Populus tremuloides*

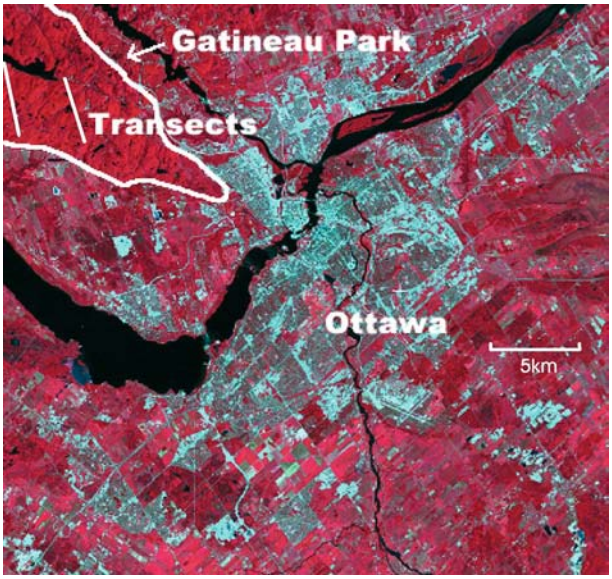

Figure 3. Portion of a Landsat image (colour infrared composite) showing the Gatineau Park and the two transects on which plots were located for Study 1.

Michx.), and red oak (*Quercus rubra* L.). Small numbers of red maple (*Acer rubrum* L.), American basswood (*Tilia americana* L.), ironwood (*Ostrya virginiana* (Mill.) K. Koch), white ash (*Fraxinus americana* L.), black ash (*Fraxinus nigra* Marsh.), white birch (*Betula papyrifera* Marsh.), and black cherry (*Prunus serotina* Ehrh.) are also present. The Gatineau Park was on the northern edge of the ice storm affected area, receiving up to 60 mm of freezing rain. Damage was patchy ranging from non-existent to large gaps left by multiple fallen trees and broken branches. As such, the park serves as a good site for remote sensing modelling because a wide range of damage is present and undamaged areas indicate pre-ice storm conditions. The objectives to-date have been to: (1) field measure and monitor forest damage and structural change over the next 10–20 years, and (2) determine the capability of high-resolution remote sensing in modelling of damage and structure. High-resolution imaging for this study has been conducted primarily with low cost digital cameras (King, 1995) and aerial photography.

3.1. METHODS

Seventy plots of 20×20 m were installed along two north–south transects (Figure 3) in areas of damage that ranged from none to severe. Suitable plot size was determined by experience in previous studies and by a semivariance

analysis conducted on field and remote sensing data of two Quebec Ministry of Natural Resources (QMNR) permanent sample plots (Butson and King, 1999). The number of plots was selected to provide adequate statistical power and capability to stratify the data based on forest or site characteristics. The transects and plot edges were oriented north–south to aid in flight navigation and minimize costs of data acquisition. Plot corners were surveyed using differential GPS to provide positional accuracy on the order of 0.5–1 m. This level of accuracy is critical for airborne remote sensing where image pixel sizes are small.

3.1.1. *Field Data Acquisition*

Field data were collected for dominant, intermediate and ground vegetation in 1998, 2000, and 2003. Three measures of damage were assessed. Visual health was assessed using a scoring system: 0 – healthy; 1 – slight damage such as one or two dead or broken branches; 2 – significant damage with up to half the crown broken or dead; 3 – severe damage with only one or two remaining live branches; and 4 – dead. Tree lean and spectral stress symptoms that cause leaf discolouration were incorporated as additional half point scores. This assessment procedure is subjective but generally repeatable within 10–20% (Lévesque and King, 1999). The number of broken stems (zero order) and 1st and 2nd order wounds where branches had broken were counted for about 1800 dominant trees in 1998. The amount of downed woody debris was assessed in 15 plots in 2000 using line intercept methods adapted from Canfield (1941). Two measures were estimated: the number of fallen branches and the total cross-sectional branch area. These two measures were tested in damage modelling subsequent to the other two measures to see if model improvements could be achieved. Other forest structure measurements included effective leaf area index (LAI_e), diameter at breast height (DBH), tree height, stem density, basal area, and ground vegetation cover. LAI_e was measured using hemispheric photographs (Rich, 1990) taken skyward under diffuse illumination of uniform cloud or at dusk and dawn. The photos were converted to binary format with vegetative matter, including leaves, branches, and trunks, as black and sky as white. Per cent cover and the gap size distribution were then derived from the image, the latter being converted to an estimate of LAI (ter Steege, 1993). This method does not account for clumping of vegetation that produces a non-random gap size distribution and often results in an underestimate of LAI. Hence, it is commonly referred to as "effective LAI" (LAI_e). Ground vegetation abundance was measured using line intercept methods similar to those for downed woody debris (Canfield, 1941).

3.1.2. *Image Data Acquisition and Processing*

Image data consisted of colour infrared (CIR) airborne digital camera imagery acquired in 1998 with a Kodak DCS 460 CIR camera ($3060 \times 2036 \times 12$-bit format), and 70 mm CIR photography, scanned to 4096×4096 pixel format. Ground pixel spacing was 60 cm for the former and 25 cm for the latter. Each sensor produced three spectral bands of about 100 nm bandwidth in the green, red, and near infrared (NIR) portions of the spectrum. For analyses completed to-date, the photographs were used because the digital camera imagery suffered from saturation in the tree crowns. Figure 4 is a portion of one of the scanned photos showing plot locations on one transect.

To accurately locate the study plots in the imagery, the images were geo-referenced as follows. White targets placed in the field before image acquisition and additional points of high contrast such as path or road intersections were differentially surveyed with a GPS. The image pixels corresponding to these targets and features were used as control points in a polynomial transformation to align the imagery with a UTM projection. First order polynomials were used in all cases to avoid differential scale change and warping across the image. Root mean square errors (RMSE) in this process were typically less than one pixel in magnitude. The images were then processed to reduce brightness variations caused by the bi-directional reflectance distribution function (BRDF) (Pellikka *et al*., 2000a) and optical effects (King, 1992).

Following image and field data processing, plot subscenes were extracted at their known geo-referenced locations in the imagery. Spectral and spatial

Figure 4. Portion of an airborne colour infrared 70 mm digitized photograph taken at the bottom end of the left transect in Figure 3. Plot locations on this portion of the transect are shown as Xs.

information was then generated for each plot. Spectral information included: mean brightness in digital numbers (DN) in the green, red and NIR bands and the normalized difference vegetation index {NDVI = (NIR – R)/(NIR + R)}. Spatial information included image texture and image structure measures. The texture measures were the standard deviation of the data in a given window and the co-occurrence matrix measure Contrast (Haralick *et al*., 1973). Window sizes were 3×3 pixels for these measures to capture within crown textures. Image structure measures included the fractions of shadow and sunlit crowns. They were determined using unsupervised ISODATA spectral cluster analysis (Jensen, 1996), a modification of the standard *k*-means statistical clustering algorithm. These spatial measures had been found in previous work to be well related to LAI_e and damage in the boreal forest (Olthof and King, 1997; Olthof and King, 2000).

3.1.3. *Image Modelling of Forest Damage*

Regression modelling of damage was then conducted in the following steps. (1) Linearity between field (y) and image (x) variables was checked. In health score modelling the shadow variable had to be logarithmically transformed. (2) Correlations between all image and damage variable pairs were produced to evaluate the image variables with highest potential for damage prediction. (3) Stepwise regression was implemented to determine the best models of a given damage variable using the set of available image variables. The significance of the F value to enter a variable in a model was set at 0.05. The parameters of interest are: R^2, the amount of variance in the field variable accounted for by the model; Adjusted R^2 (R^2_{adj}), which accounts for the reduced degrees of freedom when x variables are added to the model and is a good means for comparison of models with different numbers of x variables; the significance of the model (p) and of each variable in the model; the standard error of estimate (S_e), which measures the dispersion of measured values from the predicted model in the units of the y variable. Model residuals, were checked for normality and uniformity when plotted against y. Multicollinearity amongst independent (x) variables was checked by specifying a maximum variance inflation factor of 10 (Hocking, 1996) and by analysing paired correlations to ensure that no two x variables in the model had linear correlations (r) of greater than 0.85.

3.2. RESULTS

3.2.1. *Field Data Analysis*

Table I summarizes the significant relations between the two primary damage measures and forest structure measures. The first two columns are post-storm canopy measures indicating that greater damage was associated with reduced

Table I. Significant Pearson correlations between two of the primary damage measures and forest structure

	LAI_e	Crown closure (%)	DBH (cm)	Crown diameter (m)
Total broken stems, 1st and 2nd order wounds	−0.50**		0.68**	0.29*
Visual health score	−0.28*	−0.65**	0.27*	

Broken stems and wounds are the plot averages per dominant tree to remove effects of varied stem density between plots.

LAI_e and crown closure. The third and fourth columns essentially represent pre-storm data as DBH was not affected by the storm, and crown diameter was measurably reduced only for the most severely damaged trees. These data show that larger trees were more susceptible to damage and agree with results of Rhoads *et al.* (2002). However, relations between damage and tree height were non-significant. Figure 5 shows the scatter plot for DBH and the total number of broken stems, 1st and 2nd order wounds.

Other results obtained from the 1998 field data show that the visual damage score increased with increasing elevation ($r = 0.28$, $p < 0.05$) and that damage was greater on slope aspects facing east through to southwest than on northern slopes (t-test, $p < 0.01$). This agrees with Rhoads *et al.* (2002) who found greater damage on south facing slopes and at higher elevations, although their study elevations were higher than those of the Gatineau Park. Damage also varied according to species. For example, species such as sugar maple and red oak, with average scores of 1.79 and 1.82, respectively, were significantly less damaged (t-test, $p < 0.01$) than species

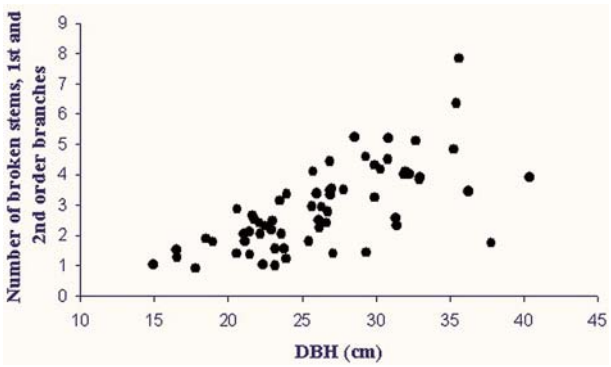

Figure 5. Relation of plot average number of broken stems, 1st order and 2nd order wounds with average tree diameter at breast height (DBH).

such as basswood and black cherry with average scores of 2.64 and 2.76, respectively. Again these results agree with those of other studies (e.g., Rhoads *et al.*, 2002). In 2000, repeat assessment of 830 dominant trees and 1142 intermediate trees found that the average score had improved significantly by 0.52 and 0.26, respectively ($p < 0.01$). Thus, most damaged trees had produced significant foliage using resources within the tree and the additional available light. The new crowns of highly damaged trees, however, were typically narrow and vertically thick in 2000. Initial analysis of the 2003 data has shown that a number of trees that had scores of 2 and 3 in 1998 had died. Also, the average relative diameter growth between 1998 and 2003 decreased with increasing damage. Trees with moderate and severe damage averaged only 5.05 and 3.1% growth in DBH, respectively, while trees that were slightly damaged or not damaged averaged DBH growth of 6.6 and 6.4%. It remains to be seen whether this trend will continue and result in more widespread premature decline and mortality.

3.2.2. *Image Modelling of Forest Damage*

Stepwise regression image modelling was conducted using the following four damage variables: the visual crown condition score, the total number of broken stems and broken branch wounds, downed wood area, and downed branch counts. Table II shows the significant model results. Downed branch

Table II. Significant multiple regressions between damage measures and airborne image variables

Model	R^2	Adjusted R^2	SE	Predictor significance	Overall significance
# Downed branches per plot					
NIR	0.77	0.71	29.5	0.03	0.00
ST. DEV. NIR				0.02	
RED				0.03	
Health score (0–4)					
LG-SHADOW$_T$	0.60	0.51	0.26	0.15	0.00
NDVI				0.00	
NIR$_{TEX}$				0.24	
GREEN				0.00	
GREEN$_{TEX}$				0.02	

Health score model is reproduced from Pellikka *et al.* (2000b). GREEN, RED, NIR = brightness in these spectral bands; ST. DEV. = standard deviation in a 3×3 window for the given band; LG = logarithmic transform of the given data; SHADOW$_T$ = transitional shadow on crown edges; NDVI = normalized difference vegetation index as defined in text; TEX = texture of the given spectral band.

count was modelled using mean plot NIR brightness, the standard deviation of the NIR band in a 3 × 3 window and mean red brightness. The model was highly significant but the standard error was 28.4% of the mean number of fallen branches per plot of 103.9 (range was 57–290). The health score was significantly modelled using mean NDVI, mean green brightness, the shadow fraction and texture in the NIR and green bands (this model is reproduced from Pellikka *et al*., (2000b)). The standard error was 12.7% of the mean health score of 2.05 (health score range = 1.19–2.82). Significant models were not produced for broken stem and branch wound counts, nor for downed wood area.

4. Study 2: Regional Scale Mapping of Forest Ice Storm Damage

The ice storm had a significant impact on maple syrup producers as production declined markedly in 1998 (Kidon *et al*., 2001), prompting the OMNR to initiate a study of treatment effects on maple health and production (Lautenschlager and Nielsen, 1999). Thirty-eight study blocks were installed and GPS surveyed in sugar maple forests of varying management and damage conditions in eastern Ontario. Figure 6 shows the block locations on a Landsat mosaic of eastern Ontario. The blocks were 100 × 100 m, consisting of four plots each of 50 × 50 m. In 35 blocks, each plot had been treated with fertilizer, lime, fertilizer and lime, or nothing (control). In the remaining three blocks herbicide was applied in three of the plots. Visual estimation of per cent crown loss was conducted by the OMNR in 34 blocks

Figure 6. Natural colour Landsat imagery of eastern Ontario showing the OMNR sugar maple experiment blocks used in Study 2.

for 6 focus trees per plot in 1999. The study also included assessment of root starch, sap, light conditions, soils, and ground vegetation abundance (Lautenschlager and Nielsen, 1999).

As a component of this sugar maple study, the OMNR wished to determine if a better ice storm forest damage map of eastern Ontario could be produced than the sketch map that resulted from airborne surveys immediately following the storm (Figure 1). A project was designed to integrate pre and post storm Landsat data with existing provincial or federal environmental data in modelling and classification of crown loss. The objectives of this study were to: (1) determine suitable remote sensing and environmental variables for damage analysis, (2) conduct modelling and classification of damage for eastern Ontario, and (3) compare four classifiers to determine the most appropriate one given data and processing requirements.

In addition, the OMNR had visual crown loss estimates for almost 2000 non-geo-referenced temporary sample plots (TSPs) across the region. These were used in assessment of damage mapping using interpolation techniques.

4.1. METHODS

4.1.1. *Data Acquisition and Processing*

Cloud-free summer Landsat Thematic Mapper (TM) imagery covering all of eastern Ontario was obtained by combining four scenes for the periods before (pre) and after (post) the storm. The pre-storm data consisted of two July 18, 1996 scenes and two July 30, 1997 scenes. The post-storm data were comprised of two August 2, 1998 scenes, one September 10, 1998 scene and one July 3, 1999 scene. Each scene was first geo-referenced using GPS data collected in 1999. Three scenes for each period (pre and post storm) were radiometrically matched to a master scene by applying linear functions relating stable land features in image overlap areas. A mosaic for each data set was then produced as shown in Figure 6. Each mosaic was atmospherically corrected with the 6S algorithm (Vermote *et al.*, 1997) using aerosol optical depth data from the nearest Aerocan sun tracking photometer station and sensor gain and offset from the master image. This converted pixel radiance into surface reflectance for each of the six TM bands (TM 1–5 and 7). The post storm mosaic was then aligned to the pre storm mosaic.

The reflectance data were stratified into deciduous and coniferous forest types using both an OMNR WoodArea GIS polygon layer, which had been interpreted from 1 : 10,000 photography, and an unsupervised cluster map of water, open, cropland, deciduous and coniferous forest generated from the Landsat data using the ISODATA algorithm (Jensen, 1996). An additional variable, distance to forest edge was extracted from this thematic map, as aerial and field observation had shown more severely bent trees at forest edges than in forest interiors. A digital elevation model (50 m grid) obtained

from the provincial 1 : 10,000 database was transformed to derive slope and aspect surfaces. Accuracy of spot heights in the DEM was 0.1 m horizontally and 1.25 m vertically. Freezing rain amounts were obtained for 284 stations from Environment Canada. A map of freezing rain was interpolated using kriging with 30 m pixels to match the Landsat pixel spacing.

For parametric classifiers, data must be normally distributed. Input data consisting of the individual spectral bands, NDVI, pre/post storm ratios of individual bands and NDVI, elevation, and precipitation were determined to be sufficiently normal, while proximity to forest edge had to be logarithmically transformed. Aspect was not included in these classifiers because of its circular nature. Slope was also not included as it was highly related to elevation in the study area and could not be transformed to a normal distribution.

4.1.2. *Damage Modelling and Classification*

The goal of this study was to produce a damage map for eastern Ontario. Initially, regression modelling of crown loss as a continuous variable was conducted as in Study 1 with the intention of applying a model derived from sample locations to all deciduous forests in the area of data coverage. Subsequently, classification of damage as an ordinal variable was conducted. In classification, crown loss was considered as three classes: none to slight damage (0–25% crown loss), moderate damage (26–50%), and high damage (>50% crown loss). They were selected to divide the data into classes of approximately equal sample size, and because they had been used in other studies of the OMNR ice storm project. The high damage class has been associated with expected growth suppression and mortality as described earlier.

Classification to produce damage maps was conducted using a common supervised data preparation procedure described in texts (e.g., Jensen, 1996). It included extraction of one training pixel from each plot, processing to determine training class statistics for parametric classifiers or to train the neural network classifier, and application of the classifiers to produce damage maps. Four classification techniques were evaluated and compared: multiple regression followed by aggregation of the predicted damage values into the three damage classes, discriminant analysis, maximum likelihood, and neural networks. Discriminant analysis seeks $k-1$ discriminant functions, where k is the number of classes to differentiate. These functions are linear combinations of the predictor variables that give the greatest amount of squared difference between groups relative to the variance within groups (Lachenbruch, 1975). All available normally distributed variables were input to the regression and discriminant analyses. The maximum likelihood classifier determines the probability density functions of each class in n dimensional

space from a set of training data, where n is the number of discriminating variables. In the classification stage, each pixel is assigned to the most likely class based on the probability density functions (Jensen, 1996). As this classifier can produce reduced accuracies when the number of input variables is high (Piper, 1992), a subset was selected that included: post storm band 3; pre/post storm ratios of bands 3 and 5; freezing precipitation; and distance to forest edge. These five variables had been identified as being the most significant contributors to the primary principal components of the data and to the multiple regression models produced prior to this analysis. A back propagation neural network (Maren *et al.*, 1980) consisting of an input layer, one hidden layer and an output layer was used. Each layer in a neural network consists of a series of nodes connected to all nodes of the layers on either side. The input training data are fed through the network and modified by sigmoid functions whose initial weights are assigned randomly. As the outputs do not match the actual classes using such weights, the error is fed back through the network and used to modify the weights. This process is repeated in many iterations until the error in output classes is below a user input tolerance. Once the network has been trained in this manner, it is used to classify the whole scene. In this study the number of iterations was 1000.

Each classifier was repetitively run 10 times using random subsets of training and test data from the total set of reference pixels in a ratio of 80 : 20. This allowed error variation to be assessed and the best classifier to be selected for production of the final damage map. This bootstrapping methodology for classification and accuracy assessment is described in detail in Olthof *et al.* (2004).

4.1.3. *Damage Interpolation from a Set of Non-Geo-referenced Temporary Sample Plot Data*

Visual estimation by OMNR staff in the nearly 2000 TSPs was very labour intensive in comparison to the data intensive procedures associated with acquisition and processing of the geo-spatial data described above. These damage estimates had potential to be used in the modelling and classification procedures but TSP locations were only approximately known from air photos or with respect to nearby roads. Consequently, extraction of geo-spatial data corresponding to the exact TSP locations was impossible and correlations between TSP damage and each of the geo-spatial variables were very poor. This highlights the necessity for field data location accuracy and spatial data geo referencing accuracy to be at least on the order of the pixel size of the spatial data.

As an alternative, the TSP data were used in interpolation to produce a damage map of eastern Ontario. Three interpolators were tested: nearest neighbour, inverse weighted distance (IDW) using an exponent of 2, and

kriging using a spherical variogram. The interpolated surfaces were evaluated for accuracy by setting aside 30 randomly selected TSP plots in three repetitions of each interpolator. RMS error was calculated for damage as a continuous variable and as a class variable.

4.2. RESULTS

Table III shows the results of stepwise regression modelling. The significant variables entered were distance to edge (−), in combination with post storm Landsat Band 7 (+), pre storm Band 1 (−), post storm Band 3 (+), and elevation (+). Distance to edge and post storm band 7 contributed equally to the adjusted R^2 (0.16 each), while the remaining three variables contributed much less (0.05, 0.02, 0.02, respectively). The model shows that damage increases closer to forest edges and at higher elevations, both trends having been observed in the field. Landsat Band 7 reflectance (mid infrared) is known to respond to variations in moisture content (Lillesand and Kiefer, 1999). It typically increases as moisture decreases, thus the positive post storm relation here shows lower biomass and/or water stress. However, interpretation is not simple as atmospheric moisture and other factors can influence the signal. Band 3 (red) responds to chlorophyll absorption and increases with reduced chlorophyll content. The positive relation of post storm red reflectance with damage in this model confirms this. Band 1 (blue) normally responds to pigments in foliage and is typically lower for healthier vegetation. In this model, its negative relation with damage is difficult to interpret.

Despite some straightforward relations with distance to forest edge and elevation, the model incorporates only a small amount of variance from one pre storm spectral band. Thus, the contribution of the temporal Landsat dataset to modelling damage seems limited. Post-storm spectral bands showing spatial variations in vegetation related to the spatial distribution of

Table III. Significant multiple regression model between damage and Landsat/environmental variables

Model	R^2	Adjusted R^2	SE (%)	Predictor significance	Overall significance
Per cent crown loss					
Dist to Edge	0.44	0.41	14.9	0.00	0.00
Post B7				0.00	
Pre B1				0.00	
Post B3				0.00	
Elev				0.00	

Dist to Edge = distance of the pixel to a forest edge; Pre = Pre storm; Post = Post storm; B7, B1, B3 = bands 7, 1, 3 of Landsat TM; Elev = elevation.

damage (amongst other factors) are all that are needed. Consequently, it was concluded that model quality, interpretation, and potential reproducibility were not adequate for mapping, so a classification approach was implemented giving the results described below.

4.2.1. *Damage Classification*

For purposes of damage mapping, the OMNR required a map of three damage classes. In each of the 10 runs of each classifier, the training and test data were assessed for accuracy. The average and range of accuracies are listed in Table IV.

The neural network classifier outperformed all other classifiers in average accuracy and in almost every individual classification run. However, its accuracies were more variable than those of the other classifiers. This is most likely due to the different training samples used in each run, and to the initial random weights of the network as additional runs with the same training data gave different classifications. Given that it was obviously the best classifier and that it varied significantly from run to run, it was decided to generate the final damage map from the mode of the 10 neural network classifications. The mode map error matrix for test plots not used in the training process is given in Table V. Overall accuracy was 77%, producer's

Table IV. Average and range of damage classification accuracies of the training and test data for four classifiers

	Training data accuracy (%) (Mean/range)	Test data accuracy (%) (Mean/range)
Regression	55/10	51/31
Maximum likelihood	72/10	55/17
Discriminant analysis	62/19	52/26
Neural network	94/25	65/35

Table V. Error matrix for the mode of the ten neural network classifications

Neural network damage class mode	Field damage class				
	1	2	3	Total	User's accuracy (%)
1	5	0	0	5	100%
2	4	8	0	12	67
3	1	2	10	13	77
Total	10	10	10	30	77
Producer's accuracy (%)	50	80	100		77

accuracy (100% – %errors of commission) varied between 50 and 100%, and the user's accuracy (100% – %errors of commission) varied between 67 and 100%. The low producer's accuracy for damage class 1 may be due to the low number of training plots that were available for this class (5–8) as 10 plots had been set aside to provide equivalent test sample size to the other two classes.

4.2.2. *Interpolated Damage Map from Temporary Sample Plot Data*

The three interpolators applied to the TSP data performed approximately equally. RMS error in per cent crown loss was similar amongst the methods, being between 15.5 and 15.6%. When the data were aggregated to the three damage classes, overall classification accuracies were: 57% – IDW; 54% – kriging; 52% – nearest neighbour. None of the producer's or user's accuracies was better than the corresponding accuracies of the neural network classification. Thus, in one-time assessment, this labour intensive procedure is probably adequate to provide a coarse estimate of crown loss and spatial representation of damage in the weeks immediately following the storm. However, to develop understanding of factors affecting damage, and to provide capability for longer-term GIS database analysis, the geo-spatial methods presented here should be more effective.

5. Summary Discussion

Two research studies have been implemented to model and map temperate forest damage following a severe ice storm. Defining a robust, objective and repeatable measure of damage is difficult. Most studies use visible crown loss or a crown condition score as subjective measures. In this research, they were used in addition to more objective measures of broken branch wounds, fallen woody debris counts and cross-sectional area.

Multiple regression modelling of damage with high-resolution airborne imagery has produced models of high significance, moderate standard error, but low to moderate variance accounted for. These models aided in identifying image parameters that respond to structural variations. For example, the integrated response of ground and understory vegetation to opening of the overstory canopy affects the remote sensing signal. As greater light penetrates damaged canopies, shadow brightness increases, the proportion of deep shadow decreases (Seed and King, 2003), textures typically increase and spectral brightness changes. These effects are currently being studied through analysis of vertical profiles of LAI_e and closure derived from hemispheric photography taken at heights up to 12 m in the canopy. This local scale study, being in an unmanaged forest, can also be used to study long-term

impacts. There is very little conclusive research on these, but expert opinion amongst the practitioners in the OMNR and QMNR suggests that strong foliage production in the first years after the storm may be followed by decline or mortality at younger than normal tree ages. Initial analysis of 2003 field data is confirming this trend. Future research will include a temporal image analysis to determine if measured canopy changes can be estimated, and continued data acquisition to refine the image models of damage and structure and to develop understanding of the long-term response of this forest to the ice storm. In addition, a canonical correlation damage modelling procedure applied by Olthof and King (2000) in the boreal forest will be adapted to attempt to assess forest structure condition in a multivariate integrated score representing various forest structure parameters.

In the regional scale study, modelling with a variety of remote sensing and environmental data types was not as fruitful but did demonstrate (expected) associations of damage with Landsat red and mid IR reflectance, distance to forest edge, and elevation. Relations of damage with the variety of forest management practices and intensities of this study have not yet been evaluated explicitly, but there is some initial evidence that intense maple syrup or other management that retains large trees and high spacing is more susceptible to damage (e.g., the DBH-damage relation (Figure 5) from the local scale study of this paper). Mapping of forest structure and damage at a regional scale may therefore provide spatial information that could aid in development of management guidelines. Average accuracy of over 75% was achieved using the mode of multiple neural networks. This was much better than the 55% average accuracy achieved using interpolation from damage estimates that had been made in a large network of TSPs across the region. The geo-spatial damage mapping methods are also more objective, repeatable, and of greater expected accuracy than the airborne sketch mapping procedure that was implemented by the OMNR immediately following the ice storm. In particular, the geo-spatial methods have the potential to be further refined and provide an archived spatial database from which greater understanding of spatial patterns and factors affecting damage can be developed.

In concurrent research to this study, forest productivity response measured by the change in LAI_e in the four summers following the storm has been found to be highly related to the damage sustained (Olthof *et al.*, 2002). In addition, as damage visually appeared to have been greater in agricultural areas than in regions of more continuous forest, evaluation of relations of landscape fragmentation to damage is being conducted. Initial tests of several fragmentation metrics have thus far shown damage to be related to patch isolation.

Acknowledgements

Funding for Study 1 was provided by the Natural Sciences and Engineering Research Council of Canada (NSERC), the National Geographic Society of the United States, the Academy of Finland and the Finnish Kordelin Foundation. Funding for Study 2 was provided by the Governments of Canada and Ontario under the Canada – Ontario Agreement for the Ice Storm Economic Recovery Assistance Program, Annex A, Assistance for the Agricultural Sector and Rural Communities in Eastern Ontario. The Canada Centre for Remote Sensing graciously provided the Landsat imagery. The OMNR Information Technology Services Branch acquired the aerial photography and digital camera imagery. Special appreciation is extended to R.A. Lautenschlager of the OMNR for support and scientific advice in Study 2, and to Doug Cameron, Yota Cosmopoulos, Janet Langdon, Steve Miles, and Steve Robbins for assistance in field data collection and analysis. Figure 1 was provided courtesy of the OMNR.

References

Aber, J. D., and Mollillo, J. M.: 1991, *Terrestrial Ecosystems*, Saunders College Publishing, Philadelphia.

Boulet, B., Trottier, F., and Roy, G.: 2000, *Management of Ice Storm Damaged Stands*, Quebec Ministry of Natural Resources, Quebec City, ISBN: 2-550-35993-3, 65 pp.

Bowers, W. W., Franklin, S. E., Hudak, J., and McDermid, G. J.: 1994, Forest structural damage analysis using image semivariance, *Can. J. Remote Sens.* **20**, 28–36.

Butson, C., and King, D. J.: 1999, Semivariance analysis of forest structure and remote sensing data to determine an optimal sample plot size, In: *Proc. 4th Int. Airborne Rem. Sens. Conf.*, Ottawa, Ontario, 21–24/06, Env. Res. Inst. of Michigan, Ann Arbor. Vol. II, pp. 155–162.

Canadian Council of Forest Ministers: 1995, Defining sustainable forest management: a Canadian approach to Criteria and Indicators, Can. For. Serv. Pub. Fo-75-3/4-1995, Ottawa, Canada.

Canadian Institute of Forestry: 2000, Forests and Climate Change, CIF Position Paper, Can. Inst. of Forestry, Ottawa, Canada.

Canfield, R.: 1941, Application of the line intercept method for sampling vegetation, *J. For.* **39**, 388–394.

Coons, C. F.: 1999, Effect of ice storm damage and other stressors on sugar bush health and sap productivity-literature review and synthesis, Eastern Ontario Model Forest Information Report, Kemptville, Ontario, 77 pp.

Coops, N. C., Stone, C., Culvenor, D. S., and Old, K.: 2001, Forest vitality and health: Indicators of changes in fundamental ecological processes in forests based on eucalypt crown condition index (ECCI), For. and Wood Prod. Res. and Dev. Corp. (FWPRDC) PN99.814, CSIRO, Canberra, ACT.

Cosmopoulos, Y. and King, D. J.: 2004, Temporal analysis of forest structural condition at an acid mine site using multispectral digital camera imagery, *Int. J. Remote Sens.* **25**, 2421–2440.

Ehrlich, P. R.: 1995, The scale of the human enterprise and biodiversity loss, In: J. H. Lawton and R. M. May (eds.), *Extinction Rates,* Oxford University Press, pp. 214–226.

Franklin, S. E.: 2000, *Remote Sensing for Sustainable Forest Management,* Lewis, New York.

Frohn, R. C.: 1998, *Remote Sensing for Landscape Ecology: New Metric Indicators for Monitoring, Modeling, and Assessment of Ecosystems*, Lewis, NY.

Goodenough, D. G., Bhogal, A. S., Fournier, R., Hall, R. J., Iisaka, J., Leckie. D., Luther, J. E., Magnussen, S., Niemann, O., and Strome, W. M.: 1998, Earth observation for sustainable development of Forests (EOSD), In: *Proc. 20th Can. Sym. Rem. Sens.*, Calgary, Alberta, 10-13/05, Can. Rem. Sens. Soc., Ottawa, pp. 57–60.

Hall, R. J., Titus, S. J., and Volney, W. J . A: 1993, Estimating top-kill volumes with large-scale photos on trees defoliated by the jack pine budworm, *Can. J. For. Res.* **23**, 1337–1346.

Haralick, R. M., Shanmugam, K., and Dinstein, I.: 1973, Textural features for image classification, *IEEE Trans. Sys. Man. Cyb.* **3**, 610–621.

Hocking, R. R.: 1996, *Methods and Applications of Linear Models: Regression and the Analysis of Variance*, Wiley and Sons, Toronto.

Hooper, M. C., Ari, K., and Lechowicz, M. J.: 2001, Impact of a major ice storm on an old-growth hardwood forest, *Can. J. Bot.* **79**, 70–75.

Irland, L. C.: 1998, Ice storm 1998 and the forests of the Northeast, *J. For.* September 1998, 32–40.

Jakubauskas, M. E.: 1996. Canonical correlation analysis of coniferous forest spectral and biotic relations, *Int. J. Remote Sens.* **17**, 2323–2332.

Jensen, J. R.: 1996, *Introductory Digital Image Processing: A Remote Sensing Perspective*, Prentice-Hall, Englewood Cliffs N.J.

Kidon, J., Fox, G., McKenney, D., and Rollins, K.: 2001, Economic impacts of the 1998 ice storm on the Eastern Ontario maple syrup industry, *For. Chron.* **77**, 667–675.

King, D. J.: 1992, Evaluation of radiometric quality, statistical characteristics and spatial resolution of multispectral videography, *J. Im. Sci. Tech.* **36**, 394–404.

King, D. J.: 1995, Airborne multispectral digital camera and video sensors: a critical review of system designs and applications, *Can. J. Remote Sens.* **21**, 245– 273.

King, D. J.: 2002, Forest structure, health and regeneration assessment using airborne digital camera imagery. In: *Proc. ForestSat Symp.*, Edinburgh, 5–9/08, UK Forestry Commission, Forest Research, Edinburgh, CD-ROM publication, 10 p.

Lachenbruch, P. A.: 1975, *Discriminant Analysis,* Hafner Press, New York.

Lautenschlager, R. A. and Nielsen, C.: 1999, Ontario's forest science efforts following the 1998 ice storm, *For. Chron.* **75**, 633–641.

Leckie, D. G., Yuan, X., Ostaff, D. P., Piene, H., and Maclean, D. A.: 1992, Analysis of high resolution multispectral MEIS imagery for spruce budworm damage assessment on a single tree basis, *Remote Sens. Environ.* **40**, 125–136.

Lévesque, J., and King, D. J.: 1999, Airborne digital camera image semivariance for evaluation of forest structural damage at an acid mine site, *Remote Sens. Environ.* **68** , 112–124.

Lévesque, J., and King, D. J.: 2003, Spatial analysis of radiometric fractions from high-resolution multispectral imagery for modelling forest structure and health, *Remote Sens. Environ.* **84**, 589–602.

Lillesand, T. M., and Kiefer, R. W.: 1999, *Remote Sensing and Image Interpretation*, 4th ed, John Wiley and Sons Inc., New York.

Mageau, M. T., Costanza, R., and Ulanowiscz, R. E.: 1995, The development and initial testing of a quantitative assessment of ecosystem health, *Ecosyst. Health* **4**, 201–213.

Maren, A. J., Harston, C. T., and Pap, P. M.: 1980, *Handbook of Neural Network Computing Applications*, Academic Press, San Diego.

Oliver, C., and Larson, B.: 1996, *Forest Stand Dynamics*, Wiley and Sons, Toronto.

Olthof, I. and King, D. J.: 1997, Evaluation of textural information in airborne CIR digital camera imagery for estimation of forest stand leaf area index, In: *Proc. 1st N. Am. Symp. on Small Format Aerial Photography*, Cloquet, Minnesota, 14-17/10, ASPRS, Bethesda, Maryland, pp. 154–164.

Olthof, I., and King, D. J.: 2000, Development of a forest health index using multispectral airborne digital camera imagery, *Can. J. Remote Sens.* **26**, 166–176.

Olthof, I., King, D. J., and Lautenschlager, R. A.: 2002, Overstory and Understory Leaf Area Index as Indicators of Forest Response to Ice Storm Damage, *Ecol. Indicators* **3**, 49–64.

Olthof, I., King, D. J., and Lautenschlager, R. A.: 2004, Evaluation of the potential to map deciduous forest ice storm damage using Landsat satellite and environmental data. *Remote Sens. Environ.* **89**, 484–496.

OMNR: 1997, Bioindicators of forest sustainability: Development of a forest condition rating system for Ontario. For. Res. Inf. Paper 137.

Parker, W. C., Colombo, S. J., Cherry, M. L., Flannigan, M. D., Greifenhagen, S., McAlpine, R. S., Papadopol, C., and Scarr, T.: 2000, Third millennium forestry: what climate change might mean to forests and forest management in Ontario, *For. Chron.* **76**, 445–463.

Peddle, D. R., Hall, F. G., and LeDrew, E. F.: 1999, Spectral mixture analysis and geometric optical reflectance modeling of boreal forest biophysical structure, *Remote Sens. Environ.* **67**, 288–297.

Pellikka, P. K. E., King, D. J., and Leblanc, S. G.: 2000a, Quantification and removal of bidirectional effects in aerial CIR imagery of deciduous forest using two reference land surface types, *Remote Sens. Rev.* **19**, 259–291.

Pellikka, P. K. E., Seed E. D., and King, D. J.: 2000b, Modelling deciduous forest ice storm damage using CIR aerial imagery and hemispheric photography, *Can. J. Remote Sens.* **26**, 394–405.

Piper, J.: 1992, Variability and bias in experimentally measured classifier error rates. *Pattern Recogn. Lett.* **13**, 685–692.

Rich, P. M.: 1990, Characterizing plant canopies with hemispherical photographs, *Remote Sens. Rev.* **5**, 13–29.

Rhoads, A. G., Hamburg, S. P., Fahey, T. J., Siccama, T. G., Hane, E. N., Battles, J., Cogbill, C., Randall, J., and Wilson, G.: 2002, Effects of an intense ice storm on the structure of a northern hardwood forest, *Can. J. For. Res.* **32**, 1763–1775.

Sampson, P. H., Mohammed, G. H., Zarco-Tejada, P. J., Miller, J. R., Noland, T. L., Irving, D., Treitz, P. M., Colombo, S. J., and Freemantle, J.: 2000, The Bioindicators of Forest Condition Project: a physiological, remote sensing approach, *For. Chron.* **76**, 941–951.

Sampson, P. H., Treitz, P. M., and Mohammed, G. H.: 2001, Remote sensing of forest condition in tolerant hardwoods: examination of spatial scale, structure and function. *Can. J. Remote Sens.* **27,** 232–246.

Seed, E. D., and King, D. J.: 2003, Shadow Brightness and Shadow Fraction Relations with Effective LAI: Importance of Canopy Closure and View Angle in Mixedwood Boreal Forest. *Can. J. Remote Sens.*, Special Issue on Measurement and use of leaf area index in monitoring vegetated ecosystems **29**, 324–335.

Smith, W. H.: 1998, Relation to Disease and Decay. In: Irland, L.C.: Ice Storm 1998 and the Forests of the Northeast, *J. For.*, September 1998, 36–37.

Stabb, M.: 1998, Seal of Approval, *Nat. Canada,* Summer 1998, 28–31.

ter Steege, H.: 1993, *HEMIPHOT: A Programme to Analyze Vegetation Indices, Light and Light Quality From Hemispherical Photographs*, Unpublished manual, The Tropenbos Foundation, Wageningen, The Netherlands.

Vermote, E. F., Tanré, D., Deuzé, J. L., Herman, M., and Morcrette, J.–J.: 1997, Second simulation of the satellite signal in the solar spectrum, 6S: an overview, *IEEE Trans. Geosci. Remote Sens.* **35**, 675–686.

Wulder, M. A., LeDrew, E. F., Franklin, S. E., and Lavigne, M. B.: 1998, Aerial image texture information in the estimation of northern deciduous and mixed wood forest leaf area index (LAI), *Remote Sens. Environ.* **64**, 64–76.